ChemPubSoc Europe

DOI: 10.1002/chem.201705758

CHEMISTRY A European Journal Communication

Proton Conductors

A Well-Established POM-based Single-Crystal Proton-Conducting Model Incorporating Multiple Weak Interactions

Xue-Li Cao,[a] Shuai-Lei Xie,[b] Shun-Li Li,[a] Long-Zhang Dong,[a] Jiang Liu,[a] Xi-Xi Liu,[a] Wen-Bin Wang,[a] Zhong-Min Su,[b] Wei Guan,*[b] and Ya-Qian Lan*[a]

Abstract: Three new proton conductors with simple structures based on isolated olyoxometalate anions as well as protonated imidazole and benzimidazole, namely, **NNU-6**–**8**, have been successfully prepared by hydrothermal reaction. We could control the number of proton sources by selecting different types and changing the charges of POM anions. The single crystal sample of **NNU-6** along *a*-axis shows a highest proton conductivity of $1.91\times10^{-2}\,S\,cm^{-1}$, which is two and three orders of magnitude higher than that of 2.42×10^{-4} and $8.90\times10^{-5}\,S\,cm^{-1}$ along *b*- and *c*-axes, respectively, due to the more unobstructed H-bonding network and stronger π–π stacking between benzimidazole rings as proton-transferring pathway along *a*-axis than that along b and c axes. It is a straightforward model to understand the metaphysical proton-conducting process, and this is the first time to put forward the idea that π–π stacking could assist proton transfer and be in favor of proton conduction, which has been demonstrated by calculating potential energy surfaces of proton transfer between benzimidazole molecules.

Proton-exchange membrane fuel cells (PEMFCs) as an important branch of energy development have attracted a lot of attention since they can convert chemicals into electricity with water as the only byproduct. Proton-exchange membrane (PEM) is the core component of PEMFCs.[1,2] Up until now, perfluorinated proton exchange membrane with high proton conductivity ($10^{-2}\,S\,cm^{-1}$) is the only one (e.g., Nafion) that has been applied; however, high cost and the environmental risk limit its application.[3] Hence, to explore low cost, environmental friendly and innovative PEM with high proton conductivity remains a challenge.

The ideal proton conductor material should contain a large number of mobile charge carriers (protons) and conducting media; moreover, the available proton transfer pathways are also extremely important. Since Keggin-type polyoxometalates (POMs) ($H_3PMo_{12}O_{40}\cdot29\,H_2O$) as proton conductor was first reported, the proton conductivity of POMs attracted increasing attention due to its disjunctive ionic structure composed of heteropolyanions and counter cations (H^+, H_3O^+, $H_2O_5^+$, etc.) could exhibit extremely high proton mobility and the oxygen-rich surface can supply more proton transfer sites in order to construct unobstructed hydrogen bond network for preferable proton transmission.[4–11] More recently, several groups have turned their energy to POM-based complexes, which probably integrate the functional characteristics of POMs and coordinated ligands to achieve synergistic effects and obtain more favorable proton-conducting properties.[10,12] Up until now, some beautiful POM-based complexes with appreciable proton conductivity have been reported, such as $(TMA)_{14}H_2[Ce^{III}(H_2O)_6]\{[Ce^{IV}{}_7Ce^{III}{}_3O_6(OH)_6(CO_3)(H_2O)_{11}][(P_2W_{16}O_{59})]_3\}\cdot41\,H_2O$, in which three dilacunary Dawson units of $[P_2W_{16}O_{59}]^{12-}$ trapped the largest Ce cluster in all the Ln-containing POM chemistry to date. However, the complicated structure led to an elusive proton-conducting process,[10a] and there are still many people confused about the relationship between crystal structure and proton-conducting property. Hence, small functional guest molecules (e.g., imidazole, triazole, histamine, etc.) that could supply mobile protons were introduced to decorate POMs in order to obtain crystallize material with simple structure and desirable proton conductivity, which should be employed to display the distinct proton-conducting process and the relationship between structure and property.[13] Consequently, some functional N-containing ligands were introduced to decorate POMs due to the protonated N-containing ligands could provide more mobile protons and help constructing unimpeded proton-transfer passage. Some compounds had been obtained and proton conductivities had been measured in detail, and the hydrogen-bonding network has been exhibited; however, the clear proton-conducting process and the relationship between proton conductivity and structure have not been analyzed systematically.[14] Furthermore, in addition to H-bonding, whether or not other weak interactions (such as π–π stacking) could be used as the pathway for proton transfer has not yet been investigated.

[a] Dr. X.-L. Cao, Prof. S.-L. Li, L.-Z. Dong, Dr. J. Liu, X.-X. Liu, W.-B. Wang, Prof. Y.-Q. Lan
School of Chemistry and Materials Science
Nanjing Normal University
Nanjing 210023 (P. R. China)
E-mail: yqlan@njnu.edu.cn

[b] S.-L. Xie, Prof. Z.-M. Su, Prof. W. Guan
Department of Chemistry
Northeast Normal University
Changchun 130024 (P. R. China)
E-mail: guanw580@nenu.edu.cn

Supporting information and the ORCID identification number(s) for the author(s) of this article can be found under https://doi.org/10.1002/chem.201705758.

According to the above points, the crystal materials with simple and well defined structure should be employed to analyse the proton-conducting process. Hence, we selected the simplest Stranberg-type POMs and the commonest Keggin-type POMs as well as small molecules of N-containing ligands (imidazole and benzimidazole) as fundamental building units for protonated N-containing ligands not only could supply more mobile protons but also help to construct proton transfer pathway. Moreover, these combinations may be able to offset the instability of POM under high relative humidity condition. In addition, it is easy to form stacking between benzimidazole or imidazole rings. More importantly, we could control the number of proton sources by selecting different types and changing the charges of POM anions. Consequently, three new proton conductors have been obtained, namely, $[P_2Mo_5O_{23}][C_7H_7N_2]_6{\cdot}H_2O$ (**NNU-6**), $[PMo_{12}O_{40}][C_7H_7N_2]_3{\cdot}2H_2O$ (**NNU-7**) and $[PMo_{11.04}V_{0.96}O_{40}][C_3H_5N_2]_4{\cdot}H_2O$ (**NNU-8**). They contain different numbers of proton sources due to including different types POM anions with different charges. These compounds all feature a simple structure. The powder sample of **NNU-6** shows a highest proton conductivity of 1.21×10^{-3} S cm^{-1} compared with that for **NNU-7** and **NNU-8** (6.87×10^{-6} and 4.45×10^{-3} S cm^{-1}, respectively), owing to the more proton sources in **NNU-6**. Hence, the single crystal of **NNU-6** was grown on a millimetre scale and showed a highest proton conductivity of 1.91×10^{-2} S cm^{-1} along *a*-axis, which is two orders of magnitude higher than that of 2.42×10^{-4} and 8.90×10^{-5} S cm^{-1} along *b*- and *c*-axis, respectively. Herein, the syntheses, crystal structures, proton conductivities as well as the relationship between crystallize structure and the different proton-conducting performances along different axes are represented.

NNU-6 crystallizes in chiral space group $P2_12_12_1$ (No. 19). It features the simplest structure composed of the Stranberg-type POMs of $[P_2Mo_5O_{23}]^{6-}$(P_2Mo_5), protonated benzimidazole and dissociative H_2O, which are connected to form a three- dimensional (3D) framework by hydrogen bonds and π–π stacking among benzimidazole rings. The asymmetrical unit contains one P_2Mo_5, six protonated benzimidazoles and one H_2O molecule (Figure 1). All building units are interconnected by hydrogen bonding. Neighboring P_2Mo_5 groups are linked by benzimidazole-4 (**B-4**), benzimidazole-5 (**B-5**) and the H_2O via N(7)–H(7)···O(7), N(8)–H(8)···O(19), N(9)–H(9)···O(22), N(10)–H(10)···O(5), O(1W)–H(1WA)···O(14) and O(1W)–H(1WB)···O(18) bonds to form a 1D $\{[P_2Mo_5O_{23}][C_7H_7N_2]_2{\cdot}H_2O\}^{4-}$anionic chain along *a*-axis (Figure S3a and S3b). Both above neighboring anionic chains are connected by benzimidazole-1 (**B-1**), benzimidazole-2 (**B-2**) and benzimidazole-3 (**B-3**) via N(1)–H(1)···O(3), N(2)–H(2)···O(1W), N(3)–H(3)···O(20), N(4)–H(4)···O(1), N(5)–H(5)···O(11) and N(6)–H(6)···O(2) bonds to form a $\{[P_2Mo_5O_{23}][C_7H_7N_2]_5{\cdot}H_2O\}^{-}$double chain down the *a*-axis, and crystal structure (Figure S3c and S3d). The average H···A and D···A distances in the structure lie in the ranges of 1.761–2.508 Å and 2.627–3.035 Å, respectively (Table S2). Moreover, there are π–π stacking among **B-1**, **B-2**, **B-3** rings along *a*-axis and **B-4**, **B-5** rings along *b*-axis (closest distance, 3.613 Å) (Table S5), which makes the connection between the building units become much stronger and then a more stable compound.

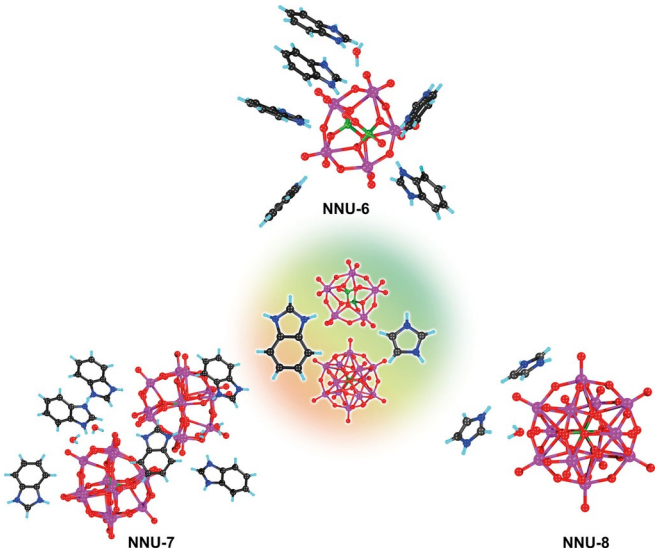

Figure 1. The asymmetric units of NNU-6, NNU-7 and NNU-8. Mo, P, C, N, H and O atoms are drawn as pink, green, gray, blue, cyan and red circles, respectively.

Each P_2Mo_5 group is surrounded by six protonated benzimidazoles and one H_2O molecule with H-bonding. All benzimidazoles are two-connected nodes. **B-2**, **B-3**, **B-4**, **B-5** and **B-6** are employed to connect two P_2Mo_5 groups, whereas **B-1** connects one P_2Mo_5 group and one H_2O molecule. Bond valence calculations on **NNU-6** gave values of 5.94–6.05 and 4.92–4.93 for Mo and P atoms, indicating that they are in oxidation states of +6 and +5, respectively.[15]

Both **NNU-7** and **NNU-8** feature the simple structure, too. The asymmetrical unit for **NNU-7** contains two Keggin-type POMs $[PMo_{12}O_{40}]^{3-}$(PMo_{12}), six protonated benzimidazoles and four H_2O molecules, whereas the asymmetrical unit for **NNU-8** contains half a Keggin-type POM $[PMo_{11.04}V_{0.96}O_{40}]^{4-}$($PMo_{11.04}V_{0.96}$), two protonated imidazoles and one H_2O molecule (Figure 1). In **NNU-7**, POMs and protonated benzimidazoles are connected to each other via H-bonding and π–π stacking to form 2D layer structure, whereas in **NNU-8**, OMs and protonated imidazoles are connected to form 3D network (Tables S3, S4, S6 and S7, Figures S4 and S5 in the Supporting Information).

It is imperative to measure the proton conductivities of the three compounds due to the proton-rich N-containing ligands and unobstructed H-bonding network. All proton conductivities were obtained from alternating current (AC) impedance spectroscopy. The conductivity of powder samples of the compounds were measured at 25 °C with different humidity to explore the varying regularity of the conductivity with the humidity rising (Figure S9a). The results show that the conductivities rise from 10^{-8}–10^{-9} S cm^{-1} at 40% RH to 10^{-4}–10^{-5} S cm^{-1} at 98% RH, which indicates that the high humidity is a positive factor for the conductivity as water molecules could supply more mobile proton transfer sites.

The temperature dependence of the proton conductivities for powder samples were measured in the temperature range of 25–50 °C (Table 1, Figure S9b). With the increase of tempera-

Table 1. The proton conductivities at 50 °C and 98% RH for samples.

Sample	Direction	Proton conductivity at 50 °C and 98% RH [S cm^{-1}]
powder sample	**NNU-6**	1.21×10^{-3}
	NNU-7	6.87×10^{-6}
	NNU-8	4.45×10^{-4}
NNU-6 single crystal	along *a*-axis	1.92×10^{-2}
	along *b*-axis	2.42×10^{-4}
	along *c*-axis	8.90×10^{-5}

ture, the optimized proton conductivity was observed to be 1.21×10^{-3} S cm^{-1} for **NNU-6**, which is three and one orders higher than that of 6.87×10^{-6} S cm^{-1} and 4.45×10^{-4} S cm^{-1} for **NNU-7** and **NNU-8**, respectively. The reason is the structure of **NNU-6** bases on Stranberg-type POMs with six negative charges, leading to more protonated benzimidazoles as proton source in **NNU-6** (Figure S9c). The activation energy was determined from least-squares fits of the slopes to obtain insight into the proton-conduction mechanism (Figure S9d). At 98% RH, the yield activation energy values (E_a) are 0.24, 0.69 and 0.40 eV for **NNU-6**, **NNU-7** and **NNU-8**, respectively.[16,17] According to previous reports about proton-conducting mechanism, the E_a in the range of 0.1–0.4 eV indicates the proton-conducting behavior occurs through a Grotthuss mechanism in **NNU-6** and **NNU-8**, whereas the E_a in 0.5–0.9 eV exposes the Vehicle mechanism is favorable for explaining the proton-conducting process in **NNU-7**.[18] Moreover, the structural integrity of the compounds was confirmed by the PXRD patterns before and after impedance analyses. (Figure S1).

To better understand the pathway the proton transport occurred, we selected **NNU-6** as a model due to its highest proton conductivity compared with **NNU-7** and **NNU-8**. Hence, we grew a large single crystal for **NNU-6** to measure the conductivities along different crystallographic axes at 25–50 °C and 98% RH. Along all axes, the proton conductivities are temperature-dependent. At 50 °C and 98% RH, the highest conductivity of 1.91×10^{-2} S cm^{-1} was obtained along *a*-axis, which is one order of magnitude higher than that of the pellet sample (Figure 4c). In the same conditions, the proton-conducting measurements along *b*- and *c*-axis yielded a maximum conductivity of 2.42×10^{-4} and 8.90×10^{-5} S cm^{-1}, respectively, which are two or three orders smaller than that obtained along the *a*-axis (Figure 2A–2C). The large differences of proton conductivities should be attributed to the different proton-conducting pathways along *a*-axis, *b*-axis and *c*-axis, which are closely related with different H-bonding networks and π–π stacking interactions among benzimidazole rings within crystal structure.

To deeply investigate the proton-conducting process and the relationship between the proton conductivities and the crystal structure, the H-bonding network and π–π stacking among benzimidazole rings in **NNU-6** have been portrayed in detail with the length of H-bonds shorter than 2.6 Å and the distance among benzimidazole rings in range of 3.613–4.528 Å (Table S2 and S5, Figure 3A, 3B and 3C). Along *a*-axis, the H-bonding could assist the proton to transfer smoothly along the double chain stretching direction accompanying the high proton conductivity along *a*-axis (Figure 3B-1). Besides, π–π stacking among **B-1**, **B-2**, **B-3** rings along *a*-axis could also encourage the proton transfer, which would further improve the proton conductivity along *a*-axis (Figure 3C-1). Along *b*- and *c*-axis, the proton-transferring in the 1D $\{[P_2Mo_5O_{23}][C_7H_7N_2]_5\cdot H_2O\}^-$double chain is unobstructed; however, the proton could only transport along the sole pathway of O(5)···H(12)-N(12)-N(11)-H(11)···O(7) between neighboring double chains, resulting in the low proton-transferring efficiency and the lower proton conductivities than that along *a*-axis (Figure 3B-2). Moreover, π–π stacking among **B-4**, **B-5** rings along *b*-axis could promote the proton transfer, resulting in the higher proton conductivity along *b*-axis than that along *c*-axis due to there are no π–π stacking among benzimidazole rings but only H-bonding to deliver proton along *c*-axis for the long N6—N7 distance of 9.13 Å (Figure 3C-2).

In addition, at 98% RH, the activation energy values (E_a) for the single crystal along *a*, *b* and *c*-axis were measured to 0.86, 0.75 and 0.53 eV, which indicate the proton-conducting behavior occurs through a Vehicle mechanism (Figure S10), which may be related with the little water adsorption capacity for single-crystal sample (Figure S11). According to water adsorption measurement, the powder sample can absorb much more

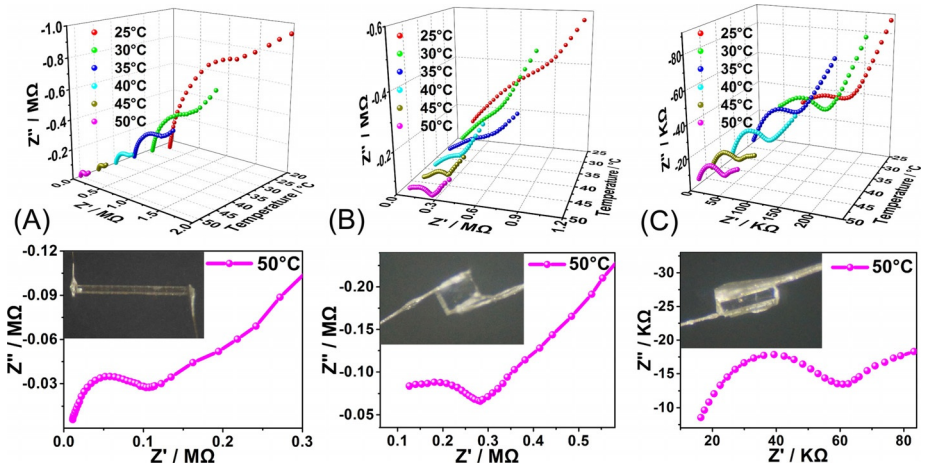

Figure 2. Impedance spectrum for single crystal of **NNU-6** at 98%RH with different temperature along *a*-axis (A), *b*-axis (B) and *c*-axis (C).

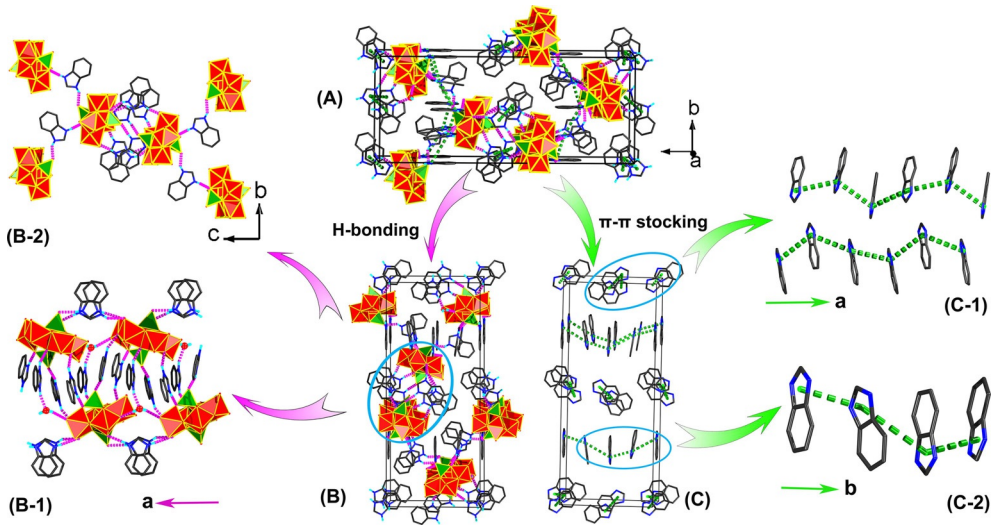

Figure 3. The H-bonding and π–π stacking among benzimidazole rings in unit cell of **NNU-6** (A); The H-bonding in unit cell (B, B-1 and B-2), and the H atoms on C atoms were delete for clarity; The π–π stacking among benzimidazole rings in unit cell (C, C-1 and C-2), and the H atoms in benzimidazole rings and the B-6 (no participation in π–π stacking) were removed for clarity.

H_2O molecules, which could be used as the sites for proton transfer, hence, the activation energy for proton-transfer in the powder sample is quite low at 0.24 eV. However, the single crystal sample can only absorb few H_2O molecules compared to powder sample, resulting in fewer sites for proton transfer, which leads to the higher activation energy for proton-conducting in single crystal sample.

In the Vehicle mechanism, the difficulty of proton transfer will determine the proton conduction ability. So we indirectly evaluate the proton conductivity by the energy barrier (ΔE) of proton transfer. The smaller the energy barrier is, the larger the proton conductivity becomes. In order to investigate the proton conduction via π–π stacking along the *a*-, *b*-, and *c*-axis directions, three simplified imidazole stacking structures $\mathbf{R_a}$, $\mathbf{R_b}$, and $\mathbf{R_c}$ were extracted from the crystal structure of **NNU-6**, as shown in Figure 4. $\mathbf{R_a}$ and $\mathbf{R_b}$ have sandwich conformations, while $\mathbf{R_c}$ is T-shaped. The rigid potential energy surfaces of proton transfer between imidazole molecules were scanned by modulating N–H bond distances and ∢N-H-N bond angles of $\mathbf{R_a}$, $\mathbf{R_b}$, and $\mathbf{R_c}$. Then, we located three proton-conductive pathways along the *a*-, *b*-, and *c*-axis directions. DFT calculations indicate that the proton conduction along the *a*-axis direction occurs via the transition state $\mathbf{TS_a}$ with the minimum ΔE value of 43.8 kcal mol^{-1}, whereas the proton conduction along the *b* and *c*-axis directions (via $\mathbf{TS_b}$ and $\mathbf{TS_c}$) require much larger ΔE values of 80.3 and 81.0 kcal mol^{-1}, respectively. Note that both $\mathbf{R_a}$ and $\mathbf{R_b}$ have the aromatic π–π stacking interaction, but the proton conduction along the *b*-axis direction is more difficult because $\mathbf{R_b}$ has a head-to-tail imidazole overlap region, in which the proton conduction takes place less readily. In addition, although ΔE values of the proton conduction along the *b*- and *c*-axis directions are similar, it can be expected that the following H3 transfer from N6 to N7 in $\mathbf{P_c}$ should become very difficult in view of long N6–N7 distance of 9.13 Å. On the basis of these results, the proton conduction ability of **NNU-6** enhances as the direction of the axis changes in the order $a > b > c$, in line with the experimental observation of the proton conductivity. In a word, it is suggested that the aromatic π–π stacking interaction caused by fully overlapping imidazole molecules significantly improves the proton conductivity.

In conclusion, we have successfully synthesized three new proton conductors containing simple POMs and small proton-

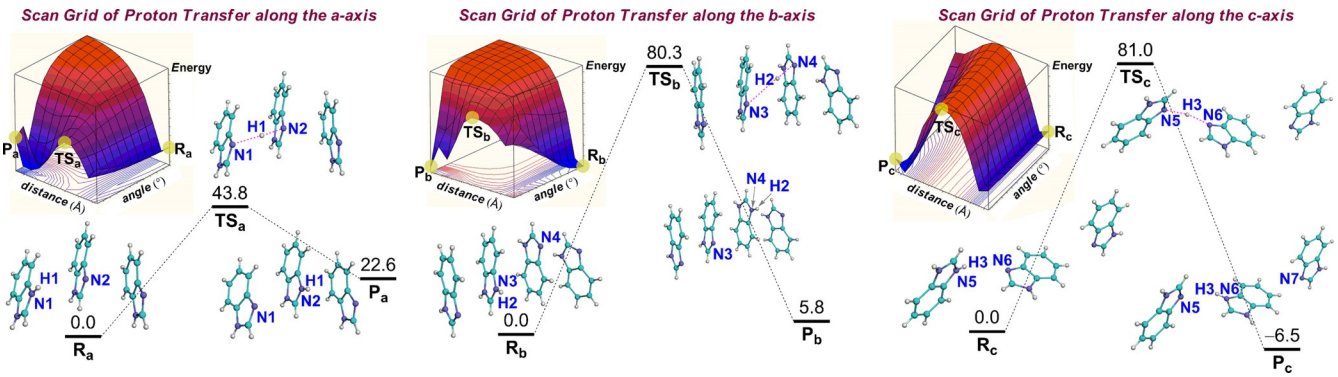

Figure 4. Scanning the potential energy surfaces of proton transfer along the *a*-, *b*-, and *c*- axis directions and energy profiles (ΔE, in kcal mol^{-1}) of three proton-conductive pathways calculated at the B3LYP-D3/6–311 + G(d,p) level in **NNU-6**.

ated N-containing ligands, namely, **NNU-6**, **NNU-7** and **NNU-8**. They all demonstrate that the protonated N-containing ligands as counter cations embrace the isolated POMs by H-bonding and π–π stacking. Also, **NNU-6** as a model was used to explore the proton-conducting pathway and process due to its structure containing more proton sources than **NNU-7** and **NNU-8**. The proton conductivity of the single crystal along *a*-axis is one of the best POM-based materials with one of the highest conductivity values reported previously, which is two and three orders of magnitude higher than that along *b*- and *c*-axis, respectively. The differences are the result of the proton-transfer along the *a*-axis via H-bonding network and π–π stacking among benzimidazole rings, which is much smoother than that along the *b*-axis and *c*-axis. Furthermore, this is the first time to put forward the idea that π–π stacking could assist proton transfer and be in favor of proton conduction, which has been demonstrated by calculating potential energy surfaces of proton transfer between benzimidazole molecules. The simple and legible crystal structure could potentially provide a convenient proton-conducting process, hopefully attracting more research devoted to proton-conducting materials.

Acknowledgements

This work was funded by the National Natural Science Foundation of China (No. 21622104, 21371099, 21701084 and 21471080), the NSF of Jiangsu Province of China (No. BK20141445), and the China Postdoctoral Science Foundation (No. 2016M590475).

Conflict of interest

The authors declare no conflict of interest.

Keywords: hydrogen bonding · N-ligand · polyoxometalates · π–π interactions · proton-conducting model

[1] a) L. Malavasi, C. A. J. Fisher, M. S. Islam, *Chem. Soc. Rev.* **2010**, *39*, 4370 – 4387; b) R. F. Service, *Science* **2002**, *296*, 1222 – 1224; c) K.-D. Kreuer, S. J. Paddison, E. Spohr, M. Schuster, *Chem. Rev.* **2004**, *104*, 4637 – 4678; d) H. Zhang, P. K. Shen, *Chem. Rev.* **2012**, *112*, 2780 – 2832; e) M. Yoon, K. Suh, H. Kim, Y. Kim, N. Selvapalam, K. Kim, *Angew. Chem. Int. Ed.* **2011**, *50*, 7870 – 7873; *Angew. Chem.* **2011**, *123*, 8016 – 8019; f) C. Laberty-Robert, K. Valle, F. Pereira, C. Sanchez, *Chem. Soc. Rev.* **2011**, *40*, 961 – 1005; g) P. Toelle, C. Koehler, R. Marschall, M. Sharifi, M. Wark, T. Frauenheim, *Chem. Soc. Rev.* **2012**, *41*, 5143 – 5159; h) D. Basak, C. Versek, D. T. Toscano, S. Christensen, M. T. Tuominen, D. Venkataraman, *Chem. Commun.* **2012**, *48*, 5922 – 5924.

[2] a) M. Yoon, K. Suh, S. Natarajan, K. Kim, *Angew. Chem. Int. Ed.* **2013**, *52*, 2688 – 2700; *Angew. Chem.* **2013**, *125*, 2752 – 2764; b) T. Yamada, K. Otsubo, R. Makiura, H. Kitagawa, *Chem. Soc. Rev.* **2013**, *42*, 6655 – 6669; c) S. L. Li, Q. Xu, *Energy Environmental Sci.* **2013**, *6*, 1656 – 1683; d) K. D. Kreuer, *Chem. Mater.* **1996**, *8*, 610 – 641; e) G. Alberti, M. Casciola, R. Palombari, *J. Membr. Sci.* **2000**, *172*, 233 – 239.

[3] Q. Li, R. He, J. O. Jensen, N. J. Bjerrum, *Chem. Mater.* **2003**, *15*, 4896 – 4915.

[4] a) M. V. Vasylyev, R. Neumann, *J. Am. Chem. Soc.* **2004**, *126*, 884 – 890; b) R. Neumann, M. Dahan, *Nature* **1997**, *388*, 353 – 355; c) N. Mizuno, A. Joonseok Min, A. Taguchi, *Chem. Mater.* **2004**, *16*, 2819 – 2825; d) K. Eguchi, I. Aso, N. Yamazoe, T. Seiyama, *Chem. Lett.* **1979**, *11*, 1345 – 1346.

[5] a) A. Müller, S. Q. N. Shah, H. Bögge, M. Schmidtmann, *Nature* **1999**, *397*, 48 – 50; b) P. Gouzerh, A. Proust, *Chem. Rev.* **1998**, *98*, 77 – 112; c) K. Binnemans, *Chem. Rev.* **2009**, *109*, 4283 – 4374; d) E. Coronadon, C. L. Gomez-Garcia, *Chem. Rev.* **1998**, *98*, 273 – 296; e) D. L. Long, R. Tsunashima, L. Cronin, *Angew. Chem. Int. Ed.* **2010**, *49*, 1736 – 1758; *Angew. Chem.* **2010**, *122*, 1780 – 1803.

[6] a) Y. Z. Zheng, M. Evangelisti, R. E. Winpenny, *Angew. Chem. Int. Ed.* **2011**, *50*, 3692 – 3695; *Angew. Chem.* **2011**, *123*, 3776 – 3779; b) J. Gao, J. Yan, S. G. Mitchell, H. N. Miras, A. G. Boulay, D.-L. Long, L. Cronin, *Chem. Sci.* **2011**, *2*, 1502 – 1508.

[7] a) J. T. Rhule, C. L. Hill, D. A. Judd, R. F. Schinazi, *Chem. Rev.* **1998**, *98*, 327 – 358; b) J. M. ClementeJuan, E. Coronado, A. Gaita-Arino, *Chem. Soc. Rev.* **2012**, *41*, 7464 – 7478; c) Y. Wang, I. A. Weinstock, *Chem. Soc. Rev.* **2012**, *41*, 7479 – 7496.

[8] D. E. Katsoulis, *Chem. Rev.* **1998**, *98*, 359 – 388.

[9] I. V. Kozhevnikov, *Chem. Rev.* **1998**, *98*, 171 – 198.

[10] a) C. Dey, T. Kundu, R. Banerjee, *Chem. Commun.* **2012**, *48*, 266 – 268; b) P. Ma, R. Wan, Y. Wang, F. Hu, D. Zhang, J. Niu, J. Wang, *Inorg. Chem.* **2016**, *55*, 918 – 924; c) S. Uchida, Y. Ogasawara, T. Maruichi, A. Kumamoto, Y. Ikuhara, T. Yamada, H. Kitagawa, N. Mizuno, *Cryst. Growth Des.* **2014**, *14*, 6620 – 6626.

[11] O. Nakamura, T. Kodama, I. Ogino, Y. Miyake, *Chem. Lett.* **1979**, *8*, 17 – 18.

[12] a) D. Wu, W. Wen, S. Chen, H. Zhang, *J. Mater. Chem. A* **2015**, *3*, 2589 – 2600; b) M. Wei, X. Wang, X. Duan, *Chemistry* **2013**, *19*, 1607; c) J. D. Halla, M. Mamak, D. E. Williams, G. A. Ozin, *Adv. Funct. Mater.* **2003**, *13*, 133 – 138.

[13] a) S. S. Nagarkar, S. M. Unni, A. Sharma, S. Kurungot, S. K. Ghosh, *Angew. Chem. Int. Ed.* **2014**, *53*, 2638 – 2642; *Angew. Chem.* **2014**, *126*, 2676 – 2680; b) V. G. Ponomareva, K. A. Kovalenko, A. P. Chupakhin, D. N. Dybtsev, E. S. Shutova, V. P. Fedin, *J. Am. Chem. Soc.* **2012**, *134*, 15640 – 15643; c) S. Liu, Z. Yue, Y. Liu, *Dalton Trans.* **2015**, *44*, 12976 – 12980; d) Y. Liu, X. Yang, J. Miao, Q. Tang, S. Liu, Z. Shi, S. Liu, *Chem. Commun.* **2014**, *50*, 10023 – 10026; e) S. Chandra, T. Kundu, S. Kandambeth, R. Babarao, Y. Marathe, S. M. Kunjir, R. Banerjee, *J. Am. Chem. Soc.* **2014**, *136*, 6570 – 6573.

[14] a) M. L. Wei, Y. X. Wang, X. J. Wang, *J. Solid State Chem.* **2014**, *209*, 29 – 36; b) M.-L. Wei, J.-H. Wang, Y.-X. Wang, *J. Solid State Chem.* **2013**, *198*, 323 – 329.

[15] a) D. Altermatt, I. D. Brown, *Acta Crystallogr. Sect. B* **2001**, *41*, 240 – 244; b) N. E. Brese, M. O'Keeffe, *Acta Crystallogr. Sect. B* **1991**, *47*, 192 – 197; c) H.-L. Jiang, F. Kong, Y. Fan, J.-G. Mao, *Inorg. Chem.* **2008**, *47*, 7430 – 7437; d) H.-L. Jiang, S.-P. Huang, Y. Fan, J.-G. Mao, W.-D. Cheng, *Chem. Eur. J.* **2008**, *14*, 1972 – 1981; e) J.-G. Mao, H.-L. Jiang, F. Kong, *Inorg. Chem.* **2008**, *47*, 8498 – 8510.

[16] O. Nakamura, T. Kodama, I. Ogino, Y. Miyake, *Chem. Lett.* **1979**, *1*, 17 – 18.

[17] K. D. Kreuer, A. Rabenau, W. Weppner, *Angew. Chem. Int. Ed. Engl.* **1982**, *21*, 208 – 209; *Angew. Chem.* **1982**, *94*, 212 – 212.

[18] P. Ramaswamy, N. E. Wong, G. K. Shimizu, *Chem. Soc. Rev.* **2014**, *43*, 5913 – 5932.

Manuscript received: December 5, 2017

Accepted manuscript online: January 5, 2018

Version of record online: January 24, 2018

